

PCCP

Accepted Manuscript



This article can be cited before page numbers have been issued, to do this please use: P. M. Quaino, G. D. Belletti, S. A. Shermukhamedov, D. V. Glukhov, E. Santos, W. Schmickler and R. Nazmutdinov, *Phys. Chem. Chem. Phys.*, 2017, DOI: 10.1039/C7CP04641C.



This is an Accepted Manuscript, which has been through the Royal Society of Chemistry peer review process and has been accepted for publication.

Accepted Manuscripts are published online shortly after acceptance, before technical editing, formatting and proof reading. Using this free service, authors can make their results available to the community, in citable form, before we publish the edited article. We will replace this Accepted Manuscript with the edited and formatted Advance Article as soon as it is available.

You can find more information about Accepted Manuscripts in the [author guidelines](#).

Please note that technical editing may introduce minor changes to the text and/or graphics, which may alter content. The journal's standard [Terms & Conditions](#) and the ethical guidelines, outlined in our [author and reviewer resource centre](#), still apply. In no event shall the Royal Society of Chemistry be held responsible for any errors or omissions in this Accepted Manuscript or any consequences arising from the use of any information it contains.

Understanding the structure and reactivity of NiCu nanoparticles: an atomistic modeling

P. Quaino^{1*}, G. Belletti¹, S.A. Shermukhamedov², D.V. Glukhov², E.Santos^{3,4}, W. Schmickler³ and R. Nazmutdinov^{2*}

¹Instituto de Química Aplicada del Litoral, IQAL (UNL-CONICET), PRELINE (FIQ-UNL), Santa Fe, Argentina

²Kazan National Research Technological University, 420015 Kazan, Republic of Tatarstan, Russian Federation

³Institute of Theoretical Chemistry, Ulm University, D-89069 Ulm, Germany

⁴Facultad de Matemática, Astronomía y Física, Instituto de Física Enrique Gaviola (IFEG-CONICET), Universidad Nacional de Córdoba, 5000 Córdoba, Argentina

*Corresponding authors

Abstract

The structure of bimetallic NiCu nanoparticles (NP) is investigated as a function of their composition and size by means of Lattice MonteCarlo (LMC) and molecular dynamics (MD) simulations. According to our results, copper segregation takes place at any composition of the particles. We found that this feature is not size-dependent. In contrast, nickel segregation depends on the NP size. While the size increases, Ni atoms tend to remain in the vicinity of the surface and deeper. For smaller NPs, Ni atoms were located at the surface as well. Our results also showed that most of the metal atoms segregated at the surface area were found to decorate edges and/or form islands. Our findings agree qualitatively with the experimental data found in the literature. In addition, we comment on the reactivity of these nanoparticles.

1 Introduction

The much (not all) energy needs and the environmental pollution problems, among many other factors, have oriented the scientific research in the recent decades toward alternative technologies e.g. fuel cells, for the generation of clean energy in order to ensure sustainable development in economic, social and environmental aspects. In this context, electrocatalysis has become a much investigated topic with an important amount of experimental and theoretical contributions, which not only explain different phenomena but predict effects and propose new electrocatalysts for the reactions.

Promising new technologies, along with some advantages of fuel cells operating in alkaline media [1, 2, 3, 4] have brought back alkaline fuel cells to the current scenario [5, 6]. Moreover, solvents are important due to their influence on the nanoparticle structure and other physical and chemical properties. For instance, they can preserve the structure of bimetallic particles during a catalytic reaction or increase the catalyst life-time. For a deeper discussion about this topic, see [7] and references therein. Nowadays, the role of the solvent and the electrode material are the most studied subjects. However, although the advance is significant, several issues are still unclear. Therefore, essential information for a rational development of electrode materials, which must be electrochemically stable and efficient in alkaline conditions, must be provided. Specifically, the design of highly active electrocatalysts for the hydrogen oxidation reaction (hor) operating at high pH has been the center of attention due to the well-known kinetic issues associated with the hor [8, 9].

Among non-noble metals, Ni seems to be a viable option as an anode for the alkaline membrane fuel cell technology because of the reduced cost and stability; although its lower activity for the hor than that of Pt [10, 11, 12] is a clear disadvantage. Hence, an improvement of the electrocatalytic properties is required. Bimetallic materials have been explored to tune the chemical properties of the electrocatalysts to modify their activity for the reaction [13, 14, 15, 16, 17, 18]. In this context, Cu seems an interesting choice to combine with Ni due to costs, corrosion stability in alkaline electrolytes and a weaker hydrogen adsorption (respect with Ni) [19]. Until now and to the best of our knowledge, good and bad activities for the hydrogen electrode reaction (HER) have been reported depending on the type of NiCu combinations, as examples see [12, 20, 21, 22].

Bimetallic catalysts in the form of nanoparticles are widely used in several areas due to their selectivity, high activity and stability. For such catalysts, an important issue is to obtain detailed description about their surface state; particularly, potential active sites in which catalysis may occur. The reactivity of bimetallic nanoparticles is significantly affected by their size, shape and composition. Hence,

the elucidation of the nanoparticle structure with the focus on the surface layers and the segregation of the components, is of paramount interest in both fundamental science and practical applications. Regarding NiCu nanoparticles, fair information can be found in the literature. Experimental work is mainly centered on the nanoparticle synthesis and their surface characterization using different techniques [12, 23, 24, 25, 26, 27], while theoretical investigations are focused on structural properties and the relation between shape, size and composition [25, 28, 29]. Although discussions about the segregation of the components of the nanoparticles is always addressed from both perspectives, theory and experiment [23, 24, 25, 26, 28, 29, 30, 31], theoretical studies oriented to that topic as well as the particle reactivity remain scarce.

Without doubts modern experimental methods are a powerful source of information for structure characterization of metal nanoparticles, but in practice the interpretation of experimental data is not straightforward. Thence, the role of computer simulations via Monte Carlo (MC) and Molecular Dynamics (MD) methods, is of great importance for clarification. In this context, the lack of understanding and information stimulates us to investigate the behavior of NiCu NPs by means of MC and MD simulations. Structure characterization of binary NiCu nanoparticles of different size and composition, as well as the effects of surface segregation have been considered. Finally, an analysis about the nanoparticle reactivity to be used as electrocatalyst for the hydrogen oxidation reaction is discussed.

2 Methodology

2.1 Monte Carlo Simulations

Atomistic Monte Carlo simulations based on the lattice model have been performed to investigate the structure of binary NiCu nanoparticles. The geometry of the particles follows the shape of a truncated fcc cube, with perfect (111) and (100) surface faces. Surface defects (steps, vacancies, kinks) were not modeled for simplicity. The MC method was used in two different versions. In the first one (lattice Monte Carlo, LMC) the lattice geometry of NPs is fixed and a selected Ni atom exchanges its position with the nearest Cu atom at each simulation step. In this method a linear interpolation was used to define interatomic separations in bimetallic systems, $r_{\text{Ni-Cu}} = x(\text{Cu})r_{\text{Cu-Cu}} + (1 - x(\text{Cu}))r_{\text{Ni-Ni}}$, where $r_{\text{Cu-Cu}}$ and $r_{\text{Ni-Ni}}$ are distances between the nearest atoms in the copper and nickel crystals. This approximation works well because the difference in the crystallographic structure of Cu and Ni is small. In the second MC version, the position of each atom in the NP was randomly shifted at each simulation step. The standard Metropolis scheme was employed; and the atomic interactions were described by the Embedded Atom Method (EAM) [32, 33], which is one of the most reliable pair potentials used in simulations for metal nanoparticles. Nanoparticles with two different effective radius values were considered: 2.2 nm (small NP), 6.6 nm (big NP). The total number of atoms was varied from 2057 to 8554. The Cu content ranged from 0.1 to 0.9 for the small NPs and 0.25 to 0.9 for the big ones. The LAMMPS code [34] was used for all the simulations. An NVT ensemble was assumed in all MC simulations; the number of steps was varied from 1.5×10^5 to 2×10^6 depending on the NP size. A value of 6.7 Å was used for the cutoff radius. Several different initial configurations of the Ni and Cu atoms (core-shell and randomly distributed) were considered in order to avoid artificial final structures. Most of the simulations were performed at room temperature.

For a more detailed analysis of the structure, we have calculated two different distribution functions (see also Ref. [25]). The radial distribution function of the metal atoms, which is defined as follows eq. 1,

$$n(r) = \frac{N_{Me}(r)}{N_{Me}^{tot}} \quad (1)$$

where $Me = \text{Cu, Ni}$; $N_{Me}(r)$ is the number of metal atoms in a spherical segment at a given $(r + \delta r)$ interval; N_{Me}^{tot} is the total number of metal atoms; and the angular distribution function, which can be defined in a similar way eq. 2,

$$n_{Me}(\theta, \varphi) = \frac{N_{Me}(\theta, \varphi)}{N_{Me}^{tot}} \quad (2)$$

where $Me = \text{Cu, Ni}$; $N_{Me}(\theta, \varphi)$ is the number of metal atoms in an angular sector restricted to $(\theta + \delta\theta)$ and $(\varphi + \delta\varphi)$. $n_{Me}(\theta, \varphi)$ exhibits the degree of heterogeneity of atom distribution on the particle volume, hence, it behaves as an indicator of island formation.

2.2 Molecular Dynamics Simulations

The binary NiCu nanoparticles have also been studied by simulated annealing followed by a classical molecular dynamic simulation at room temperature as well. The simulations were performed using OpenMD code [35] under a condition of constant temperature (NVT ensemble). The interactions between the atoms in the bimetallic clusters were described through the embedded atom method (EAM) [36]. The temperature of the system has been controlled using a Nosé-Hoover thermostat. The time step was set as 1 fs in the simulations. According to our procedure, for each cluster size, a simulated annealing has been performed wherein the temperature varies from above the melting point of the NP to room temperature with a temperature step of 20 K, where the temperature was maintained for 8 ps in each step. After the simulated annealing, a molecular dynamics at 300 K has been performed to verify constant energy and temperature (production time: 1000 ps).

For the sake of clarification, our studies have been performed by means of two well-known methods - MD and LMC - with different technical procedure: while in MC the nanoparticle geometry remains in a rigid fcc lattice, and only Ni and Cu atoms are allowed to reordered according to their energetics, the whole particle is allowed to move in the MD. Beyond the obvious differences, the general behavior should be comparable. Both in the MC and MD simulations solvent was addressed neither explicitly nor implicitly. It should be mentioned that the hydrophilic properties of the Ni and Cu surfaces do not differ much. Therefore, the solvent effect does not seem to lead to significant changes of our conclusions based on the model calculations.

3 Results and discussion

Firstly, we have investigated by MC the dependence of the structure on the composition, and as consequence surface segregation phenomena. Results corresponding to particles of 2057 atoms (diameter = 2.2 nm) and 8554 atoms (diameter = 6.6 nm) with a variable composition of (10 - 90) and (25 - 90) at. % Cu respectively are reported in this contribution. Fig. 1 and Fig. 2 show the geometries obtained for each nanoparticle size at four different compositions: 10, 20, 50, 90 at. % Cu. The selected structures are representative of all other investigated nanoparticles and compositions.

Our simulations show a remarkable surface segregation of copper atoms for the bimetallic particles at all the studied sizes and compositions. Experimental studies based on Auger Electron Spectroscopy [24], atom probe field ion microscope [31] and Low Energy Ion Scattering [37] are in accord with our results. The segregation was found to be rather symmetrical, i.e. there is no special direction pointing to more (or less) preferable sectors at the nanoparticle surface. This conclusion is supported by a detailed analysis based on the angular distribution functions.

The structure of the nanoparticles resembles a "core-shell" type, although with some specific features. This result is in agreement with theoretical and experimental evidences, which show that the configuration inside the alloys looks similar to a "diffuse" core-shell pattern [27, 29, 38]. Cu atoms are mainly distributed at the surface region, whereas Ni atoms are found inside the particles (see Fig. 1 and Fig. 2, specifically the cross sections of each NP). The explanation of this behavior is based on the energetics: a combination of two metals with an important difference in their cohesive energy favours the core formation of the metal with significantly larger cohesive energy ($\epsilon_{\text{coh}}^{\text{Ni}} = 4.44$ eV/atom $>$ $\epsilon_{\text{coh}}^{\text{Cu}} = 3.49$ eV/atom) [39] and the shell formation of the metal with relatively small surface energy ($E_{\text{surf}}^{\text{Ni}} = 2.45$ J/m² $>$ $E_{\text{surf}}^{\text{Cu}} = 1.83$ J/m²) [40]. Therefore, the cohesive and surface energies in the bimetallic nanoparticles act in the same direction and favour the Cu segregation at the NP surface. In addition, Cu-Ni positive mixing energies reported in [41] favor the segregation of Cu to the sites with lower coordination. In this context, surface segregation phenomena shows a nice dependence on the coordination of the particle sites with the copper composition. At low Cu concentration, segregation occurs preferably on the lowest coordinated sites: edges and corners (Fig. 1(a,b), Fig. 2(a) and Fig. 3). The initial segregation on the vertices and edges, which are less saturated by the nearest coordination bonds (in comparison with the faces) looks natural from the view point of enthalpy factor. This observation is in qualitative agreement with the results of MC simulations for NiCu nanoparticles of cubic shape reported earlier by Mainardi and Balbuena [28] (see more details in SI, Fig. 3S). Of course, nanoparticles consisting of 319 atoms are too small and all observations about the structure of this system are qualitative. The aim of this study is only to compare our predictions with those reported previously in [28]. In part, according to our results for cubic nanoparticles the segregation activity (i.e. the occupation of NP surface by Cu atoms) of three different faces increases in the following order: (110) $<$ (111) $<$ (331). This result agrees quite well with conclusion made by the authors in Ref. [28]: (110) $<$ (111) $<$ (331). Since the amount

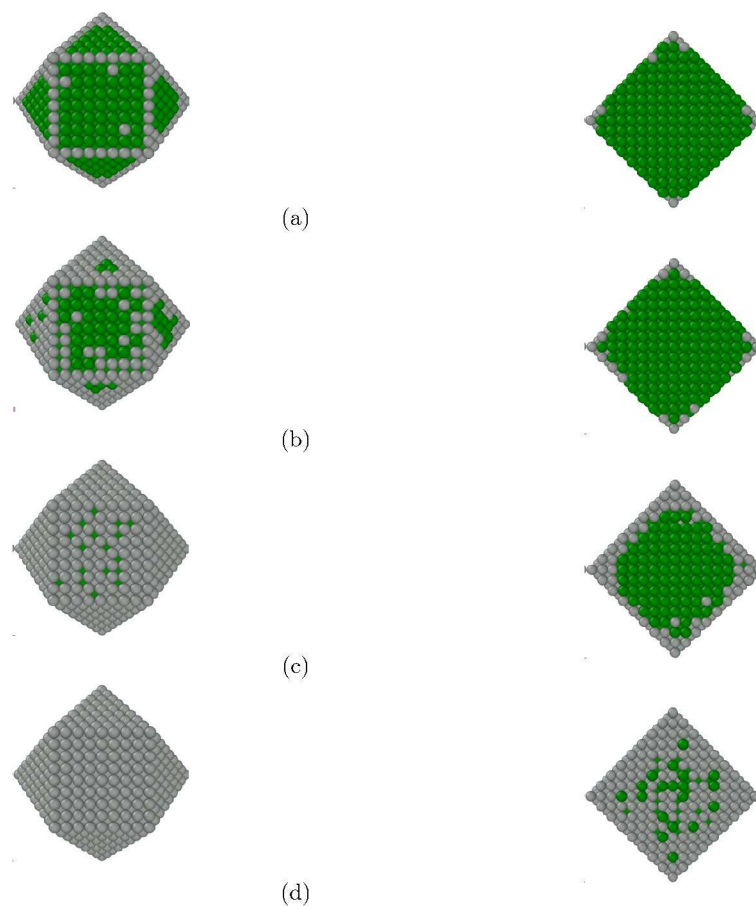


Figure 1: Three-dimensional images of nanoparticles consisting of 2057 atoms at different compositions: a) 10 at. % Cu (grey) and 90 at. % Ni (green) b) 20 at. % Cu and 80 at. % Ni c) 50 at. % Cu and 50 at. % Ni d) 90 at. % Cu and 10 at. % Ni. Left side: nanoparticle geometrical structures, right side: nanoparticle cross section.

of copper increases, the facets get "covered" with Cu atoms, only after all the borders are occupied (Figs. 1(b-d), 2(b-d) and 3). Despite the total square (S) of (100) faces that prevails in our particles ($S(100)/S(111) = \sqrt{3}$ from pure geometrical reasons), it can be readily seen in Fig. 3 that the (100) face is more active than the (111) one in the terms of segregation.

It should be noticed that this behavior is mainly observed for low Cu content ($\approx < 20\%$). For higher amounts, the particles exhibit enriched or fully covered facets (Fig. 1(c,d) and Fig. 2(c,d)). As an example, the radial and angular distributions of a particle at two different concentrations of copper are shown in Fig.4, which clearly supports our previous explanation. For completeness, the behavior of all investigated particles with configurations, cross sections and angular and radial distributions are presented in SI. As can be seen from Figs. 1S and 2S, the segregation profile of Cu is not monotonous and reveals at least one main maximum. This qualitatively agrees with the conclusions in [26, 33]. It is interesting to note that authors in [29] found a Janus-like structure for a NiCu nanoparticle ($x(\text{Cu}) = 0.5$) using MD simulations at $T = 10$ K, while we have never observed any similar structure in our model systems at no temperatures.

In addition, our results confirm that the segregation of Ni is much weaker than that of Cu. Indeed, depending on the amount of copper, this behavior is clearly identified at both studied sizes. For Cu contents $< \approx 20\%$, its amount is not enough to cover all the particle surface; then, Ni atoms are expected at the surface as well. This is a region where both Ni and Cu atoms co-exist. For higher Cu contents ($> \approx 20\%$), the particle surface is entirely occupied by copper, and no segregation of nickel atoms is detected at the surface. For instance, in a nanoparticle with 30 at.% Cu, the Ni atoms reside in the vicinity of the second layer, (see Fig. 1S in SI); similar results were reported by Wang *et al.*, where Cu surface segregation was observed, while Ni segregates to the planes below the surface [42]. Finally, at

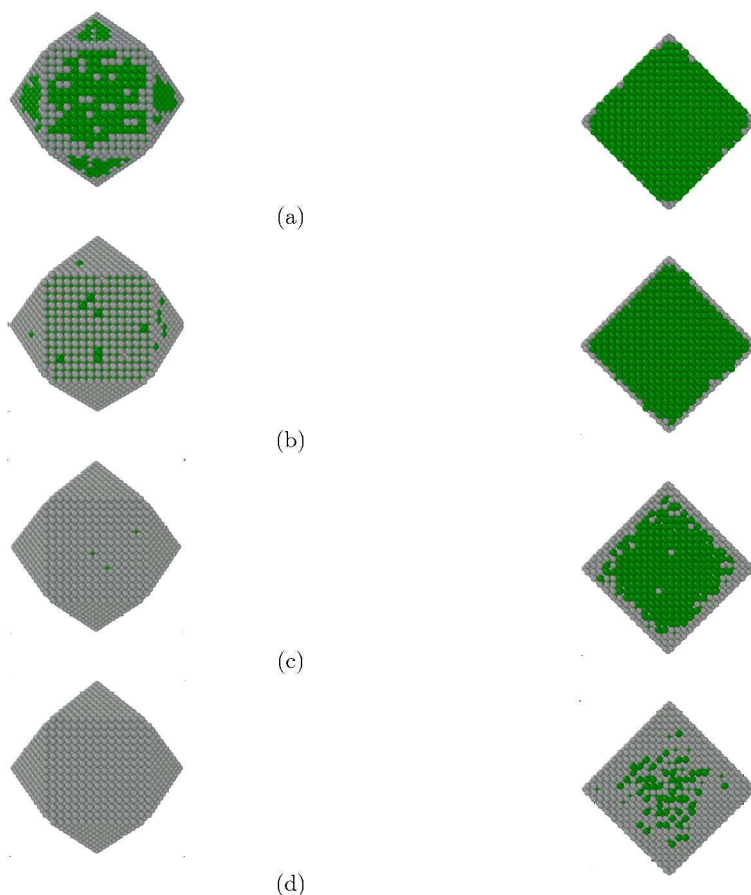


Figure 2: Three-dimensional images of nanoparticles consisting of 8554 atoms at different compositions: a) 10 at. % Cu (grey) and 90 at. % Ni (green) b) 20 at. % Cu and 80 at. % Ni c) 50 at. % Cu and 50 at. % Ni d) 90 at. % Cu and 10 at. % Ni. Left side: nanoparticle geometrical structures, right side: nanoparticle cross section.

fairly low Ni concentration, most of these atoms are found disordered in the central area of the particle (Fig. 1S and Fig. 2S in the SI). These findings are in accordance with most of the theoretical and experimental work reported in the literature [24, 31, 43]. It must be mentioned that there still exists some discrepancies between authors, some of them report oscillatory behavior in the depth profile [23, 26]. For instance, by using Ultraviolet Photoemission Spectroscopy (UPS) Ling *et al.* explained that the Cu enrichment region shows at least one oscillation [26]. At the same time other report evidence that Ni segregates at the surface of NiCu alloys at significantly low Ni concentration [30, 44]. Note that there are some differences in the computational results obtained in [25] compared with the present ones, due to different models considered to describe the interaction parameters of the Morse potentials applied in [25], which seem to overestimate the tendency of both Cu and Ni atoms in the bimetallic NPs to form island-like structures. Moreover, according to the previous results [25], Ni atoms come to the first surface layer at small Ni content in the bimetallic nanoparticles.

To support our conclusions on Ni segregation in NiCu nanoparticles, we have performed MD simulations of two NPs with different sizes and at two different temperatures, 900 K and 20 K (see SI, Fig. 4S). The initial geometry used at $T = 20$ K was previously obtained by simulations at the high temperature (900 K). Nanoparticle composition and temperature values correspond to experimental conditions using NiCu NPs as described in [45] (heated nanoparticles were sharply cooled). One can see that in all cases segregated Ni atoms are observed not farther than the second layer of the surface region, while the first surface layer is occupied by the Cu atoms. The faceted structure of the NP surface is detected as well (see SI, Fig. 4S). It can be assumed that Ni segregation observed in experiments [30, 44] might be probably treated as a non-equilibrium effect (i.e. the system needs more time to attain equilibrium).

According to our results and to shed light for a better understanding, smaller bimetallic particles have

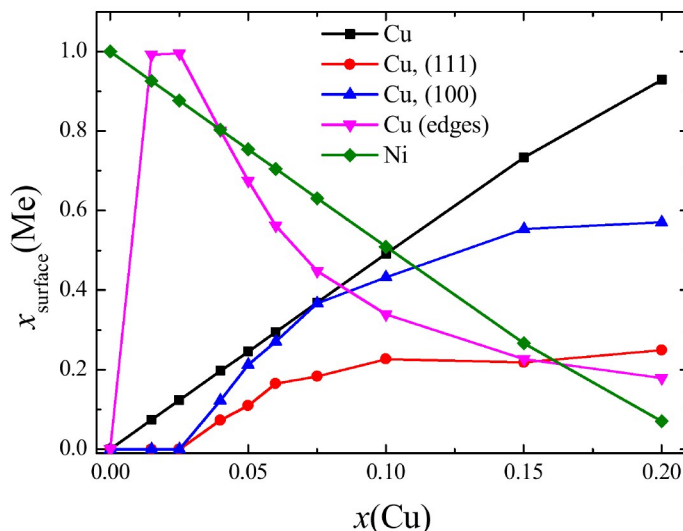


Figure 3: Dependence of the surface concentration of Cu and Ni atoms, $x_{\text{surface}}(\text{Me})$, on the total Cu fraction, $x(\text{Cu})$, in the NiCu nanoparticles. $x_{\text{surface}}(\text{Me})$ (Me=Cu, Ni) is the fraction of the Me atoms in the first surface layer of the NP and $x(\text{Cu})$ is the fraction of Cu atoms in the whole NP. The total number of atoms in the NPs is 8554.

been simulated by classical MD according to the methodology explained in Section 2.2. The particles were investigated at two copper contents of ca. 20% and 80%, and six different sizes with the following number of total atoms (N): 174, 288, 420, 540, 640, 784.

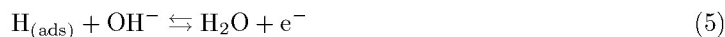
Fig. 5 and Fig. 6 show the average structures and the corresponding cross sections of both nanoparticle sets obtained by MD. As expected, and due to methodological reasons, the obtained particles show a special feature: the bond lengths between the atoms is not uniform, i.e. the particles exhibit no symmetry and no smooth surface is found.

Our results demonstrate that surface segregation of both atoms (Ni and Cu) always appears at small particle sizes (< 800 atoms), Fig. 5 and Fig. 6, bottom rows, and indicate that the surface is mainly formed by copper with a certain amount of nickel. Regardless of the proportion of Cu/Ni atoms, Cu is always detected inside the particles. Most of the Ni or Cu atoms segregated at the surface were found to form small island-like structures mixed with random distributions (Fig. 5 and Fig. 6).

Both methods show faceted particles. In MC, the particles are highly ordered and faceted by construction, while in MD the particles exhibit facets, which are not perfectly defined and quite random (Fig. 5 and Fig. 6, top rows). Finally, a common neighbor analysis [46] (Adaptative CNA method [47]) allows us to identify the structure-type of atoms distributed in the nanoparticles. Results are displayed in Fig. 7 and Fig. 8 for 20 and 80 at. % Cu, respectively. It can be seen that the smallest particle show an important disorder with increasing size, the particles tend to a higher order crystalline structure.

Particle reactivity and hydrogen oxidation reaction (hor)

It is well-known that the hydrogen oxidation reaction (hor) in alkaline media consists of the following elementary steps, Tafel (3), Heyrovsky (4), and Volmer (5):



Processes (3) and (4) are alternatives, which often compete. The reaction always evolves through an adsorbed intermediate ($\text{H}_{(\text{ads})}$) on an active site on the metal electrode. Although (OH^-) is one of the

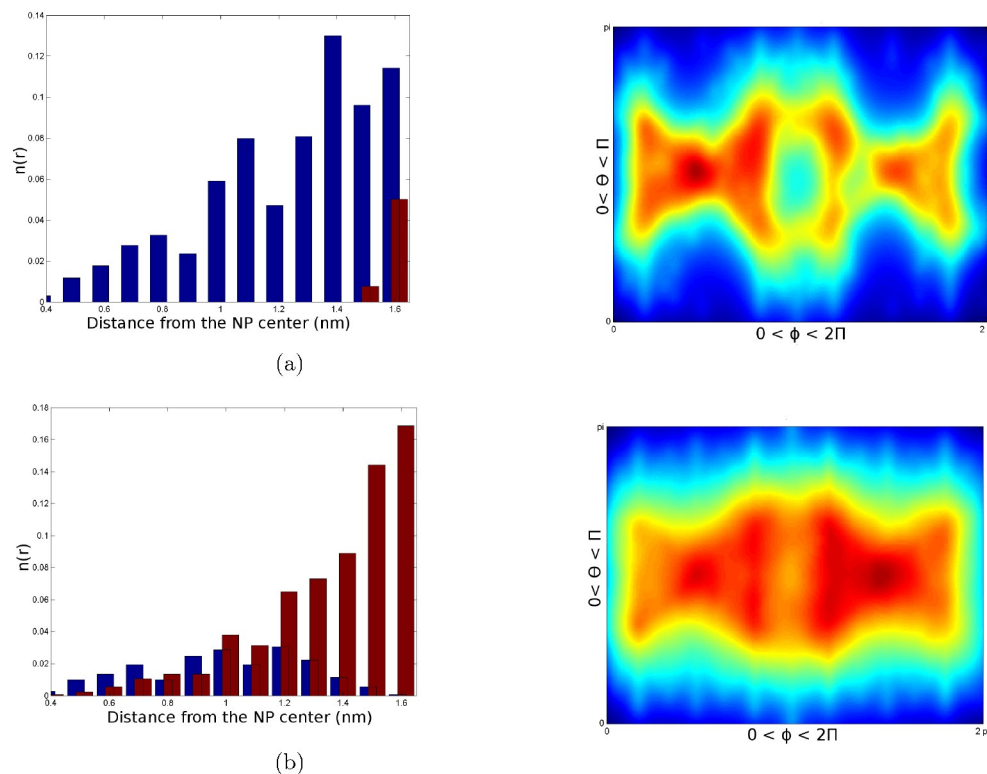


Figure 4: A nanoparticle consisting of 2057 atoms at two compositions: a) 20 at. % Cu and 80 at. % Ni b) 80 at. % Cu and 20 at. % Ni. Left side: radial distributions for Ni(blue) and Cu(bordeaux). Right side: angular distributions, red and blue colors represent high and lower content of copper, respectively.

reactants in the hor, the oxygenated species might also be produced by the electrochemical adsorption of a hydroxyl from the solution onto the surface of the metal electrode (6):



where the adsorbed species ($\text{H}_{(\text{ads})}$ and $\text{OH}_{(\text{ads})}$) will combine to generate water as a product (7).



In accord with these considerations we focus on reactions (3), (6) and (7). The reactions (3) and (6) proceed in parallel. The electrochemical step (6) is assumed to be fast due to strong orbital overlap effects, which result in decreasing the activation barrier [48], and the chemical bond breaking process (3) is most likely the rate controlling step. D. Strmcnik *et al* [14] demonstrated that the $\text{OH}_{(\text{ads})}$ is a key reactant in the hor in alkaline media, and catalysed the hydrogen oxidation reaction rate by promotion of hydroxyl adsorption. Therefore, a rational design of Ni-Cu bimetallic materials should allow to optimize the $\text{H}_{(\text{ads})}/\text{OH}_{(\text{ads})}$ energetics to tune the reaction rate.

Therefore, to understand the particle reactivity, several nickel-copper slab configurations, which might be found in the NPs, were modeled within DFT (see SI for technical details and Table 1 for modeled geometries) to evaluate the effects that influence the hydrogen adsorption and the electrocatalytic properties of the substrate. Ligand effect, due to lattice constant mismatch ($a_0^{\text{Cu}} > a_0^{\text{Ni}}$), and chemical interactions between both metals play a crucial role in the adsorption process as reported in [49]. Thus, as a first approximation, to evaluate the reactivity of the nanoparticles, the changes in the electronic structure of the bimetallic configurations were analysed. A comparison of the surface d bands for the bare and combined systems is shown in Fig. 9. The DOS of the d band changes with the combination of both metals in comparison with the pure ones. The bands appear to be shifted to more positive energies (Fig. 9: red, green and yellow lines) compared to the pure Cu surface (Fig. 9: black line). The misfit of the lattice constant induces a geometrical effect that causes a change in the electronic properties.

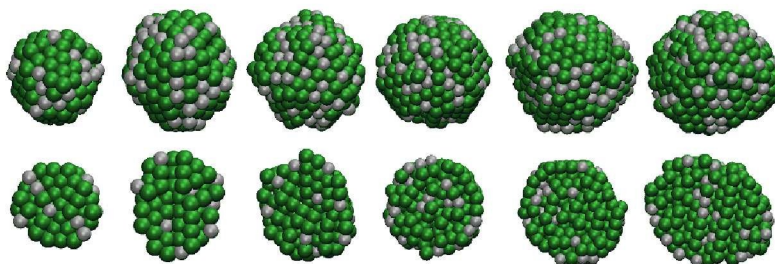


Figure 5: Average structure (top row) and cross section (bottom row) of the studied clusters. The particles in both rows follow the sequence: $\text{Ni}_{140}\text{Cu}_{34}$, $\text{Ni}_{229}\text{Cu}_{59}$, $\text{Ni}_{337}\text{Cu}_{83}$, $\text{Ni}_{434}\text{Cu}_{106}$, $\text{Ni}_{510}\text{Cu}_{130}$, $\text{Ni}_{624}\text{Cu}_{160}$. Colour references: Ni atoms are represented by green balls and Cu atoms are represented by gray balls.

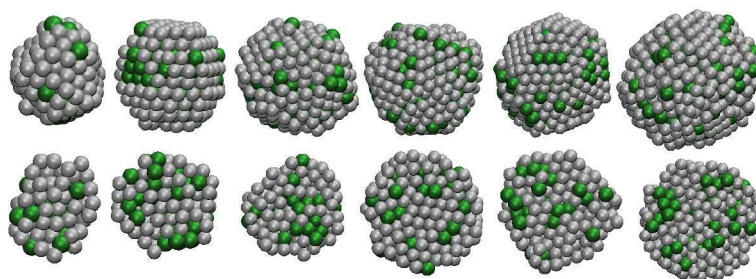


Figure 6: Average structure (top row) and cross section (bottom row) of the studied clusters. The particles in both rows follow the sequence: $\text{Ni}_{34}\text{Cu}_{140}$, $\text{Ni}_{59}\text{Cu}_{229}$, $\text{Ni}_{83}\text{Cu}_{337}$, $\text{Ni}_{106}\text{Cu}_{434}$, $\text{Ni}_{130}\text{Cu}_{510}$, $\text{Ni}_{160}\text{Cu}_{624}$. Colour references: Ni atoms are represented by grey balls and Cu atoms are represented by green balls.

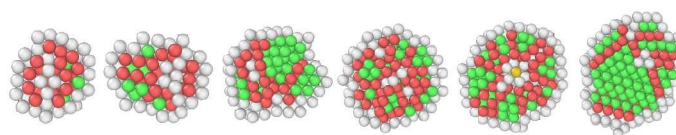


Figure 7: Common neighbor analysis [46] (Adaptative CNA method [47]). Cross section view of the NiCu clusters obtained from the MD simulations. The particles in the row follow the sequence: $\text{Ni}_{140}\text{Cu}_{34}$, $\text{Ni}_{229}\text{Cu}_{59}$, $\text{Ni}_{337}\text{Cu}_{83}$, $\text{Ni}_{434}\text{Cu}_{106}$, $\text{Ni}_{510}\text{Cu}_{130}$, $\text{Ni}_{624}\text{Cu}_{160}$. Colour references for the balls match the structure type according to: unknown coordination structure (white), fcc (green), hcp (red), others.

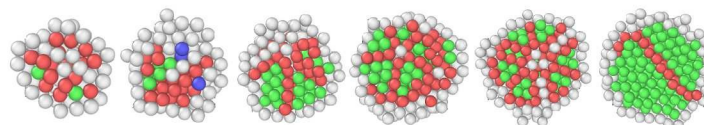


Figure 8: Common neighbor analysis [46] (Adaptative CNA method [47]). Cross section view of the NiCu clusters obtained from the MD simulations. The particles in the row follow the sequence: $\text{Ni}_{34}\text{Cu}_{140}$, $\text{Ni}_{59}\text{Cu}_{229}$, $\text{Ni}_{83}\text{Cu}_{337}$, $\text{Ni}_{106}\text{Cu}_{434}$, $\text{Ni}_{130}\text{Cu}_{510}$, $\text{Ni}_{160}\text{Cu}_{624}$. Colour references for the balls match the structure type according to: unknown coordination structure (white), bcc (blue), fcc (green), hcp (red), others.

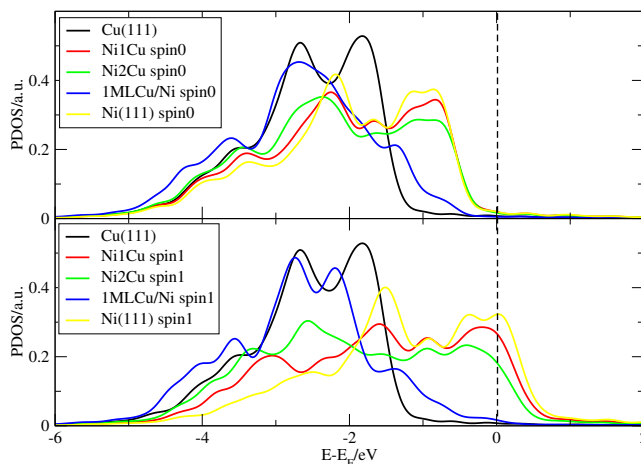


Figure 9: Density of states projected on the surface d bands for systems under study. For detailed information about each system structure (Ni1Cu, Ni2Cu, 1MLCu/Ni) see Table 1 and SI. The vertical line indicates the position of the Fermi level.

Indeed, for nanoparticles like the ones obtained in our simulations, we expect several values of lattice parameters, which are between the lattice constant of the pure metals. Moreover, the modifications in the electronic structure are a consequence of the chemical interplay due to the direct contact between nickel and copper. Then, it is expected that the d band profiles for the bimetallic structures tend to the d band of the pure metal found in higher amount (e.g. Fig. 9: black and blue lines¹). The upshift of the d bands to more positive energies and the narrower profiles might be generally associated with a higher reactivity implying an improvement of the chemisorption properties. This fact is in accordance with the values of adsorption energies for OH shown in Table 1. A similar trend was also found for the H adsorption (not shown in the present contribution).

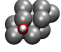
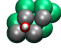
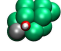
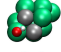

System	System identification	Adsorption stable site	E_{ads}/eV
	Cu(111)	fcc	-2.88
	1MLCu/Ni(111)	fcc	-2.98
	Ni1Cu	fcc	-3.18
	Ni2Cu	top	-3.20
	Ni(111)	fcc	-3.23

Table 1: Geometrical structures that mimic parts of the NPs. Cu atoms in grey, Ni atoms in green, O atoms in red and H atoms in white. Adsorption energies for the OH are reported for the most stable site found in each configuration.

In very recent work [50], the maximum of catalytic activity for the hydrogen oxidation reaction on the NiCu nanoparticles was observed at nearly $x(\text{Cu}) = 5\%$. As can be seen from Figs. 1-3, at this composition, all ridges and apices of the nanoparticles are occupied by the Cu atoms; further increasing of $x(\text{Cu})$ results in reducing the nickel fraction on the faces. As the reactivity of Ni in hydrogen reactions is higher as compared with copper, such observations might explain qualitatively the experimental data [50].

It is evident from Table 1, on the other hand, that bare Cu is the worst surface for adsorption, whereas pure Ni is the best one. The energetics for the Cu-Ni mixtures are found in the middle. Therefore, the

¹It is interesting to note that in the case of a ML of Cu on Ni(111), the geometrical effect is a contraction of the monolayer due to the lattice constant mismatch, where $a_0^{\text{Ni}} < a_0^{\text{Cu}}$. Therefore, geometrical effects are less pronounced, being the chemical interaction the main one. For a detailed explanation, read [49]

presence of copper atoms to the nickel structure allows the tuning of the energetics in the OH and H adsorption. It is well-known that hydrogen adsorbs stronger on Ni(111) ($\Delta G \approx -0.3$ eV) compared to Cu(111) ($\Delta G \approx 0.1$ eV) [19, 51]. On the other side, the adsorption of OH is highly favored on both metals. Even more, the heat of reaction (7) ($\Delta E = 0$ eV for Cu and $\Delta E = 0.3$ eV for Ni) and its activation barrier ($\Delta E_a = 0.68$ eV for Cu and $\Delta E_a = 0.90$ eV for Ni) have been calculated for the pure metals (for technical details see SI), and our results show that the water formation (7) on the copper surface proceeds faster and is more favorable from the viewpoint of thermodynamics.

Hence, the addition of copper atoms to Ni nanoparticles might destabilizes the hydrogen adsorption on Ni as well as the hydroxyl adsorption; and favors the combination reaction (7). The improvement should occur for low copper concentration, where both type of atoms exist on the surface (Fig. 1(a,b) and Fig. 2(a)); as the amount of Cu increases, the particle tends to resemble a core-shell type with the Cu atoms localized mostly on the surface (Fig. 1(c,d) and Fig. 2(b-d)). Since hydrogen adsorption is not favorable on pure copper [19], an attenuation in the reaction should appear compared to the Ni-Cu surface.

4 Conclusions

We found that the copper atoms in the NiCu nanoparticles exhibit a surface segregation even at very small Cu content. This feature is not size-dependent; the segregation profile along the NP radius reveals at least one maximum. In contrast the nickel segregation is strongly size-dependent. This effect disappears with increasing bimetallic nanoparticle size and the Ni atoms can reside only in the vicinity of the second surface layer and deeper. Finally the reactivity of NiCu nanoparticles in the electrochemical hydrogen oxidation results from a very delicate balance between the surface electronic structure (position of d-band with respect to the Fermi level, electronic density profile) and the adsorption energies of H and OH species. Both these factors significantly affect the rate of electrochemical and chemical steps (3)-(5). Again, nickel is more active than copper in the electrochemical step, $\text{OH}^- \rightleftharpoons \text{OH}_{(\text{ads})} + \text{e}^-$. On the other hand, in the resulting chemical stage ($\text{H}_{(\text{ads})} + \text{OH}_{(\text{ads})} \rightleftharpoons \text{H}_2\text{O}$) copper is more active as compared with nickel, i.e. provides the lower activation barrier. This is the reason why the best catalysis in the electrochemical hydrogen oxidation takes place at a certain (compromise) surface structure which results basically from the copper segregation. A more comprehensive treatment of the mechanism of hydrogen oxidation at the bimetallic nanoparticle surface should rest on a combination of the quantum mechanical theory of charge transfer with molecular modeling [52]; work which is in progress and will be addressed in a future contribution, as well a natural extension of our work to study the effect of the solvent.

Acknowledgements

This work is financed by PICT-2014-1084 and CAID 501 201101 00276 LI UNL. The authors thank the support given by the Santa Fe Science Technology and Innovation Agency (ASACTEI, grant 00010-18-2014). P.Q., E.S. and G.B. also thank UNL and CONICET for continuous support. R.N. greatly thanks the RFBR (project No 17-53-150008).

References

- [1] Varcoe J. R., Slade R. C. T., Lam How Yee E., Poynton S. D., Driscoll D. J., and Apperley D. C. *Chem. Mater.*, 19:2686–2693, 2007.
- [2] Robertson N. J., Kostalik IV H. A., Clark T. J., Mutolo P. F., Abruña H. D., , and Coates G. W. *J. Am. Chem. Soc.*, 132:3400–3404, 2010.
- [3] Hibbs M. R., Fujimoto C. H., and Cornelius C. J. *Macromolecules*, 42:8316–8321, 2009.
- [4] J. R. Varcoe and R. C. T. Slade. *Fuel Cells*, 5:187–200, 2005.
- [5] Wang Y-J, Qiao J., Baker R., and Zhang J. *Chem. Soc. Rev.*, 42:5768–5787, 2013.
- [6] Varcoe J. R., Atanassov P., Dekel D.R., Herring A.M., Hickner M.A., Kohl P.A., Kucernak A.R., Mustain W.E., Nijmeijer K., Scott K., Xu T., and Zhuang L. *Energy Environ. Sci.*, 7:3135–3191, 2014.

- [7] Dang-Bao T, Pla D., Favier I, and Gómez M. *Catalysts*, 7:1–33, 2017.
- [8] Durst J., Siebel A., Simon C., Hasche F., Herranz J., and Gasteiger H. A. *Energy Environ. Sci.*, 7:2255–2260, 2014.
- [9] Sheng W., Gasteiger H. A., and Shao-Horn Y. *J. Electrochem. Soc.*, 157:B1529–B1536, 2010.
- [10] Sheng W., Myint M., Chen J. G., and Yan Y. *Energy environ. sci.* 6:1509–1512, 2013.
- [11] Marini S., Salvi P., Nelli P., Pesenti R., Villa M., and Kiros Y. *Int J Hydrog Energy*, 38:11484–11495, 2013.
- [12] Cherstiouk O., Simonov A., Oshchepkov A., Zaikovskii V., Kardash T., Bonnefont A, Parmon V., and Savinova E. *J. Electroanal. Chem.*, 783:146–151, 2016.
- [13] Subbaraman R., Tripkovic D., Chang K., Strmcnik D., Paulikas A., Hirunsit P., Chan M., Greeley J., Stamenkovic V., and Markovic N. *Nature Materials*, 11:550–557, 2012.
- [14] Strmcnik D., Uchimura M., Wang C., Subbaraman R., Danilovic N., van der Vliet D., Paulikas A., Stamenkovic V., and Markovic N. *Nature Chemistry*, 5:300–306, 2013.
- [15] Juarez M.F., Soldano G., Santos E., Guesmi H., Tielens F., and Mineva T. *Computation*, 4:1–12, 2016.
- [16] Juarez M.F., Soldano G., Guesmi H., Tielens F., and Santos E. *Surface Science*, 4:235–247, 2015.
- [17] Zhu B., Creuze J., Mottet C., Legrand B., and Guesmi H. *J. Phys. Chem. C*, 120:350–359, 2016.
- [18] Wang L, Huang L, Jiao Ch., Huang Z, Liang F, Liu S., Wang Y, and Zhang H. *Catalysts*, 7:1–11, 2017.
- [19] Santos E., Lundin A., Pötting K., Quaino P., and Schmickler W. *Phys. Rev. B*, 79:235436(1)–235436(10), 2009.
- [20] Conway B., Beatty E., and DeMaine P. *Electrochim. Acta*, 7:39–54, 1962.
- [21] Ngamlerdpokin K. and Tantavichet N. *Int. J. Hydrog. Energy*, 39:2505–2515, 2014.
- [22] Ahn S. H., Park HH-Y., Choi I., Yoo S. J., Hwang S.J., Kim H-J., Cho E. A., Yoon C. W., Son H., Hernandez J. M., Nam S.W., Lim T-H, Kim S-K, and Jang J. H. *Int. J. Hydrog. Energy*, 38:13493–13501, 2013.
- [23] Webber P.R., Rojas C. E., and Dobson P.J. *Surf. Sci.*, 105:20–40, 1981.
- [24] Kuniaki Watanabe K., Hashiba M., and Yamashina T. *Surf. Sci.*, 61:483–490, 1976.
- [25] Oshchepkov A., Simonov P., Cherstiouk O., Nazmutdinov R., Glukhov D., Zaikovskii V., Kardash T., Kvon R., Bonnefont A., Simonov A., Parmon V., and Savinova E. *Top Catal.*, 58:1181–1192, 2015.
- [26] Ling D.T., Miller J.N., Lindau I., Spicer W.E., and Stefan P.M. *Surf. Sci.*, 74:612–620, 1978.
- [27] Avila-Davila E., Lopez-Hirata V., Saucedo-Muñoz M., and Gonzalez-Velazquez J. *Journa of Alloys and Compounds*, 460:206–212, 2008.
- [28] Mainardi D. and Balbuena P. *Langmuir*, 17:2047–2050, 2001.
- [29] Hennes M., Buchwald J., and Mayr S.G. *CrystEngComm*, 14:7633–7638, 2012.
- [30] Sakurai T, Hashizume T., Kobayashi A., Sakai A., Hyodo S., Kuk Y., and Pickering H. *Phys. Rev. B*, 34:8379–8390, 1986.
- [31] Ng Y. S., Tsong T. T, and McLane S. B. Jr. *Phys. Rev. Lett.*, 42:588–591, 1979.
- [32] Zhou X.W., Wadley H.N., Johnson R.A., Larson D.J., Tabat N., Cerezo A., Petford-Long A.K., Smith G.D., Clifton P.H., Martens R.L., and Kelly T.F. *Acta Mater.*, 49:4005–4015, 2001.

- [33] Onat B. and Durukanoglu S. *J. Phys. Cond. Matt.*, 26:035404(1)–035404(13), 2014.
- [34] Plimpton S.J. <http://lammps.sandia.gov/index.html>. *J. Comp. Phys.*, 117:1–19, 1995.
- [35] <http://openmd.org>.
- [36] Foiles S., Baskes M., and Daw M. *Phys. Rev. B*, 33:7983–7991, 1986.
- [37] Brongersma H.H and Sparnaay M.J. *Surf. Sci.*, 71:657–678, 1978.
- [38] H-Lopez V.M., Sakurai T., and Hirano K. *Scripta Metallurgica et Materialia*, 26:99–103, 1992.
- [39] C. Kittel. *Introduction to Solid State Physics*. John Wiley and Sons, Hoboken, NJ, 8th edition, 2005.
- [40] Skriver H. L. and Rosengaard N. M. *Phys. Rev. B*, 46:7157–7168, 1992.
- [41] Zhu L. and DePriesto A. E. *J. Catal.*, 167:400–407, 1997.
- [42] Wang H.J., Najafabadi R., Srolovitz D.J., and LeSar R. *Phys. Rev. B*, 45:12028–12042, 1992.
- [43] Durham P.J., Jordan R.G., Sohal G.S., and Wille L.T. *Phys. Rev. Lett.*, 53:2038–2041, 1984.
- [44] Sakurai T, Hashizume T., Jimbo A., Sakai A., and Hyodo S. *Phys. Rev. Lett.*, 55:514–517, 1985.
- [45] J.R. Anderson. *Structure of metal catalysts*. Academic Press, NY, 1975.
- [46] J. Honeycutt and H. Andersen. *J. Phys. Chem*, 91:4950–4963, 1987.
- [47] A. Stukowski. *Modell. Simul. Mater. Sci. Eng.*, 20:045021(1)–045021(15), 2012.
- [48] Pinto L.M.C., P. Quaino P., Arce M. D., Santos E., and Schmickler W. *Chem. phys. chem.* 15:2003–2009, 2014.
- [49] Santos E., Quaino P., and Schmickler W. *Electrochimica acta.* 55:4346–4352, 2010.
- [50] Cherstiouk O.V., Simonov P.A., Oshchepkov A.G., Zaikovskii V.I., Kardash T.Yu., Bonnefont A., Parmon V.N., and Savinova E.R. *J. Eletroanal. Chem.*, 783:146–151, 2016.
- [51] Greeley J., Jaramillo T.F., Bonde J., Chorkendorff I.B., and Nørskov J.K. *Nature Materials*, 5:909–913, 2006.
- [52] Nazmutdinov R.R., Bronshtein M.D., Zinkicheva T.T., and Glukhov D.V. *Int. J. Quant. Chem.*, 116:189–201, 2016.

Table of Contents

Fine details of the surface structure of NiCu nanoparticles of different size and composition are investigated by atomistic simulations. Their reactivity in the electrochemical hydrogen oxidation is discussed in terms of the density of electronic states.

